# Analysis of high reverse currents of 4H-SiC Schottky-barrier diodes

Hiroyuki Okino,[a] Norifumi Kameshiro, Kumiko Konishi, Akio Shima, and Ren-ichi Yamada
*Central Research Laboratory, Hitachi, Ltd., 1-280 Higashi-koigakubo, Kokubunji-shi, Tokyo 185-8601, Japan*

(Received 15 October 2017; accepted 1 December 2017; published online 21 December 2017)

Nickel (Ni), titanium (Ti), and molybdenum (Mo) 4H-silicon carbide Schottky-barrier diodes (SiC SBDs) were fabricated and used to investigate the relation between forward and reverse currents. Temperature dependence of reverse current follows a theory that includes tunneling in regard to thermionic emission, namely, temperature dependence is weak at low temperature but strong at high temperatures. On the other hand, the reverse currents of the Ni and Mo SBDs are higher than their respective currents calculated from their Schottky barrier heights (SBHs), whereas the reverse current of the Ti SBD agrees well with that calculated from its SBH. The cause of the high reverse currents was investigated from the viewpoints of low barrier patch, Gaussian distribution of barrier height (GD), thin surface barrier, and electron effective mass. The high reverse current of the Ni and Mo SBDs can be explained not in terms of a low-barrier patch, GD, or thin surface barrier but in terms of small effective masses. Investigation of crystal structures at the Schottky interface revealed a large lattice mismatch between the metals (Ni, Ti, or Mo) and SiC for the Ni and Mo SBDs. The small effective mass is possibly attributed to the large lattice mismatch, which might generate transition layers at the Schottky interface. It is concluded from these results that the lattice constant as well as the work function is an important factor in selecting the metal species as the Schottky metal for wide band-gap SBDs, for which tunneling current dominates reverse current. *Published by AIP Publishing*. https://doi.org/10.1063/1.5009344

## I. INTRODUCTION

In recent years, silicon-carbide Schottky barrier diodes (SiC SBDs) have attracted wide attention because they greatly reduce loss in energy-conversion systems, and large chip-size SiC SBDs are already emerging.[1] Schottky barrier height (SBH) is generally the most-important parameter concerning SBDs, so dependences of metal species, crystal structures, and crystal orientation on SBH have been studied.[2–6] SBH can be extracted from forward current-voltage (*I-V*) characteristics on the basis of thermionic-emission theory.[7] This theory is also applicable to reverse *I-V* characteristics if the electric field at the Schottky interface is low, i.e., in the order of 0.1 MV/cm. However, the superior material properties of SiC enable SiC SBDs to operate in high electric fields (in the order of 1 MV/cm); accordingly, when reverse characteristics of SiC are SBDs analyzed, tunneling must be considered.[8]

To date, due to the low material quality of SiC crystal and epi-layer, experimental studies on reverse *I-V* characteristics of SiC SBDs have mainly focused on revealing the correlation between crystal defects and electric characteristics.[9–14] Since the material quality is being improved,[15] it is becoming necessary to study the nature of reverse characteristics. Accordingly, tunneling current was numerically calculated by Crofton and Sriram using the WKB approximation. Compared with measured reverse current of a platinum/6H-SiC SBD at 300 and 373 K, the calculated tunneling current agreed better than that calculated on the basis of thermionic emission theory.[16] Moreover, tantalum, tungsten, titanium (Ti), and nickel (Ni)/4H-SiC SBDs have been fabricated by Treu *et al*., and it was shown that reverse currents at temperatures between 21 and 200 °C, which are the analytical form of tunneling current at intermediate temperatures, follow the thermionic-field emission theory.[17] And reverse currents calculated by Blasciuc-Dimitriu *et al*. using a transfer matrix successfully reproduced measured reverse currents of SiC SBDs.[18]

In this study, which attempts to reveal fundamental physics, not just the fitting of reverse currents, nickel, titanium, and molybdenum (Mo)/4H-SiC SBDs were fabricated and the dependences of those metal species on reverse current were analyzed on the basis of a theory that includes tunneling in regard to thermionic emission. The analysis results revealed that the reverse currents of the Ni and Mo SBDs are higher than those expected from the tunneling theory, whereas that of the Ti SBD agrees well with that predicted by the tunneling theory. The reverse currents are discussed from the viewpoints of temperature dependences, low barrier patch,[19,20] Gaussian distribution of barrier height (GD),[21,22] thin surface barrier,[23,24] and electron effective mass.[25,26] The high reverse currents of the Ni and Mo SBDs are explained not in terms of low barrier patch, GD, or thin surface barrier but in terms of small effective mass, which is possibly attributable to lattice mismatch between metals and SiC.

## II. METHODS

SBDs were fabricated on the Si face of 4H-SiC substrate. A schematic image of the cross-section of a fabricated SBD is shown in the inset of Fig. 2. At the periphery of the active area, the SBDs had a junction termination extension

[a]hiroyuki.okino.wj@hitachi.com

(JTE) structure fabricated by implantation of aluminum and subsequent annealing.[27] After the sacrificial oxide was removed by hydrofluoric acid, either Ti, Ni, or Mo (with thickness of 50 nm) was sputtered (as a Schottky metal) on the SiC surface, and the resulting structure was annealed at 663 K in pure $N_2$. A backside ohmic contact was fabricated by forming nickel silicide. The normal axis plane was tilted 4° from $(0001)_{SiC}$. Donor concentration of drift layers was $2.5–3.5 \times 10^{15}\,cm^{-3}$. The thickness of drift layers was 30 $\mu$m, and the area of the Schottky contacts was $0.026\,cm^2$.

The thermionic-emission theory used to extract SBH and ideality factor ($n$) from forward characteristics is expressed as[7]

$$J = A^{**}T^2 \exp(-q\phi_B/k_BT)(\exp(qV_F/nk_BT) - 1), \quad (1a)$$

$$= J_s(\exp(qV_F/nk_BT) - 1), \quad (1b)$$

where $A^{**}$ is the effective Richardson constant, i.e., 146 A/cm$^2$ K$^2$[2,3] $T$ is the temperature, $q$ is the elementary charge on an electron, $\phi_B$ is SBH, $k_B$ is the Boltzmann's constant, $V_F$ is the forward voltage, and $J_s$ is the saturation current, which is a value extrapolated from current-voltage ($I$-$V$) characteristics at $V = 0$. Conduction mechanisms under forward and reverse bias are schematically depicted in Fig. 1. Since the electric field at the Schottky interface of SiC-SBDs is high, namely, in the order of 1 MV/cm, the Schottky barrier is thin enough that tunneling current flows through the Schottky interface in the reverse mode. To calculate tunneling current, the following equation was used:[23]

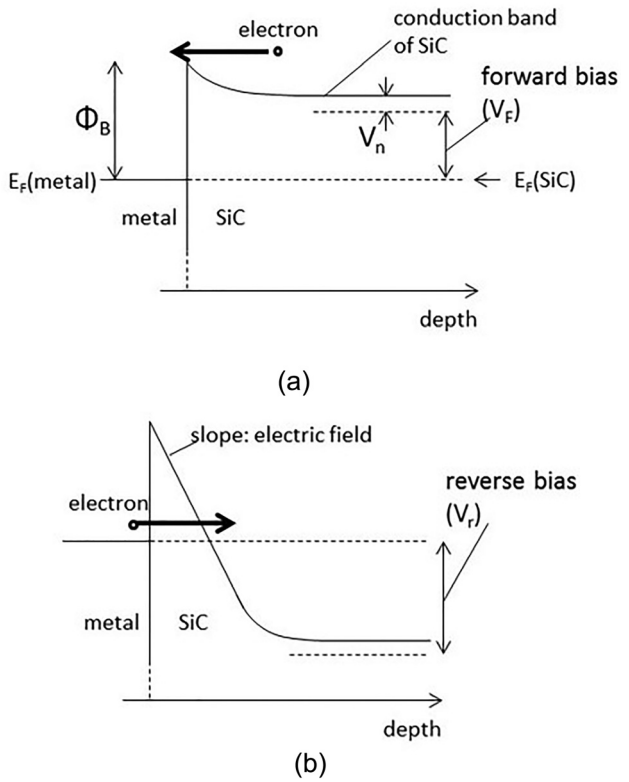


FIG. 1. Schematics of conduction mechanisms of a SBD in (a) forward state and (b) reverse state.

$$J = \frac{4\pi q m^*}{h^3}\int_0^\infty\int T(E)[f_m(E_p + E_z) - f_s(E_p + E_z)]dE_p dE_z, \quad (2)$$

where $h$ is the Planck's constant, $m^*$ is the effective mass of an electron, $T(E)$ is the tunneling probability, $E_z$ is the normal component of electron energy at the Schottky interface, $E_p$ is the parallel component of that electron energy, and $f_s$ and $f_m$ are the Fermi-Dirac distribution functions for SiC and the metals. In the derivation of Eq. (2), a parabolic relationship, such as $E_z = \hbar^2 k_z^2/2m^*$, where $k_z$ is the wave number normal to the Schottky interface, is assumed. To simplify the calculation, the same effective mass is assumed for metals and SiC. The influence of this assumption is considered in the Sec. IV. Tunneling probability $T(E)$ was calculated in accordance with the WKB approximation, given as

$$T(E) = \exp\left[-2\frac{\sqrt{2m^*}}{\hbar}\int_{z_1}^{z_2}\sqrt{\phi(z) - E_z}dz\right], \quad (3)$$

where $z_1$ and $z_2$ are the classical turning points, and $\phi(z)$ is the potential distribution. Lowering of image force is included in $\phi(z)$.[8] Note that the current in Eq. (2) contains the current component of thermionic emission. The current in Eq. (2) is thus referred to as "tunneling current" hereinafter.

By comparing the reverse current of an SBD with that of a pn diode fabricated on the same SiC wafer, thus with the same doping concentration, it was confirmed that the reverse currents of the fabricated SBDs are conducted through the Schottky interface and not through the termination region as shown in Fig. 2. Reverse $I$-$V$ characteristics of two Ti SBDs with different doping concentrations are shown in Fig. 3(a). In regard to the dependence of the electric field at the Schottky interface, as shown in Fig. 3(b), the reverse currents of the two SBDs coincide. This coincidence stems from the fact that the potential distribution is determined by the electric field at the Schottky interface, as shown in Fig. 1(b). Since the donor concentration of the SBDs varies among samples, the reverse currents of SBDs were compared in terms of electric-field dependence. In the calculation of the

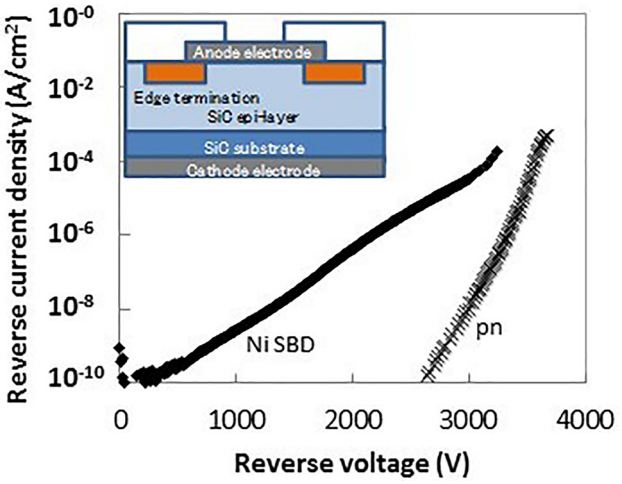


FIG. 2. Reverse characteristics of a Ni SBD and a pn diode at 298 K. (Inset: schematic cross-section of a fabricated SBD.)

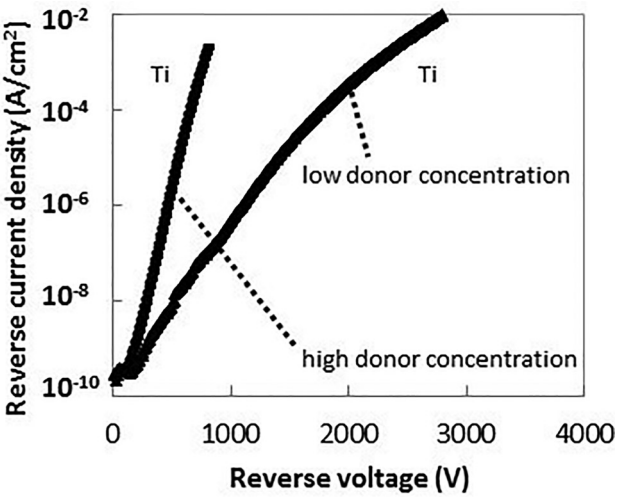


(a)

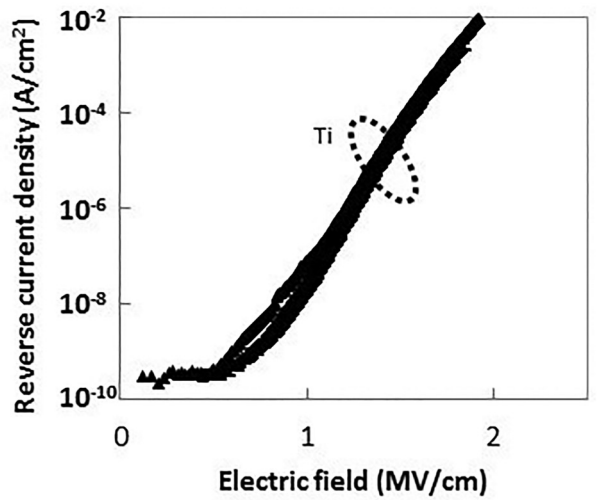


(b)

FIG. 3. (a) Reverse I-V characteristics of two Ti SBDs with different doping concentrations at 298 K. (b) Dependences of reverse characteristics of Ti SBDs on electric field. The samples are the same as those in (a).

electric field at the Schottky interface, the donor density obtained from capacitance-voltage ($C$-$V$) characteristics and a dielectric constant of 9.66 $\varepsilon_0$ were used for 4H-SiC, where $\varepsilon_0$ is the dielectric constant in a vacuum.[7]

## III. RESULTS

Forward and reverse current-voltage ($I$-$V$) characteristics of Ti, Ni, and Mo SiC-SBDs at 298 K are shown in Figs. 4 and 5. The SBHs are extracted from Fig. 4 as 1.20 (Ti), 1.60 (Ni), and 1.23 (Mo). Although the Mo SBD shows higher SBH than the Ti SBD, the Mo SBD shows higher reverse current than the Ti SBD. Dependence of reverse current on SBH at 298 K and an electric field at a Schottky interface of 1.0 MV/cm is shown in Fig. 6. The figure also shows tunneling current calculated from Eq. (2) with $m^*$ of 0.25 $m_0$, where $m_0$ is free electron mass, and a reported reverse current.[28,29] Although the conduction-band effective mass normal to $(0001)_{SiC}$ is about 0.3 $m_0$,[30,31] 0.25 $m_0$, which

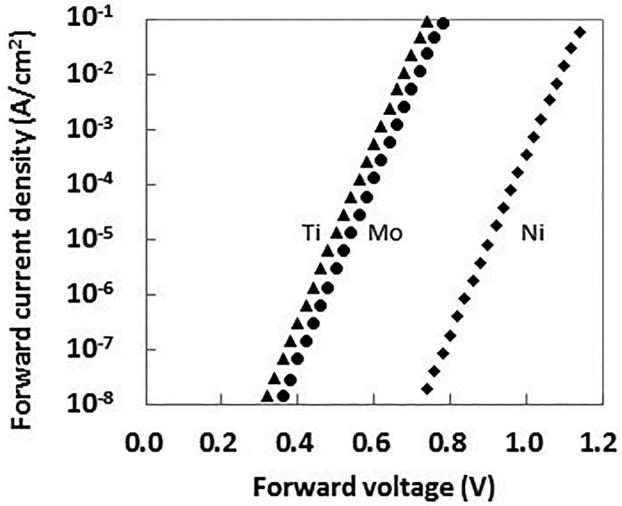


FIG. 4. Forward characteristics of SBDs at 298 K (triangles: Ti; circles: Mo; and diamonds: Ni).

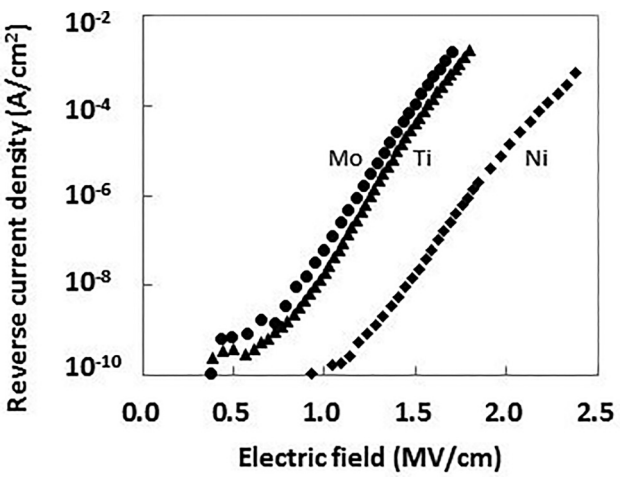


FIG. 5. Reverse characteristics of SBDs at 298 K (triangles: Ti; circles: Mo; and diamonds: Ni).

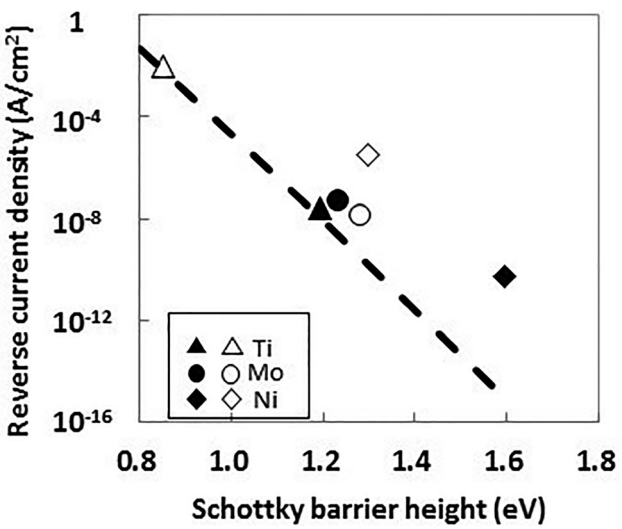


FIG. 6. Reverse-current density of SBDs at 298 K. Electric field at the Schottky interface is 1.0 MV/cm. Filled symbols represent the data measured in this study. Open symbols represent the measured data taken from the literature.[28,29] Triangles: Ti; circles: Mo; and diamond: Ni. Dashed line represents the current density calculated from Eq. (2) with the effective mass of 0.25 $m_0$.

reproduces the measured data accurately, was used. The measured reverse current of the Ti SBD and the reported reverse current of a Ti SBD agree well with the expected currents calculated from their SBHs. On the other hand, the measured reverse currents of the Mo and Ni SBDs are higher than the expected reverse currents calculated from their SBHs. The measured reverse current of the Ni SBD shows an especially large deviation from the calculated one. Since the calculation assumes the mechanism of the reverse current to be tunneling, the mechanism was investigated by considering the temperature dependence of the reverse current.

Reverse characteristics of the Ni, Ti, and Mo SBDs at various temperatures are shown in Figs. 7(a)–7(c). The corresponding temperature dependences of reverse currents are shown in Figs. 8(a)–8(c). Tunneling currents calculated from Eq. (2) with $m^*$ of 0.25 $m_0$ and thermionic emission current are also shown. The tendencies of the temperature dependence in the cases of all the fabricated SBDs are quite similar, though the measured reverse currents of the Ni and Mo SBDs are much higher than the calculated currents. The reverse currents are weakly dependent on temperature at low temperature and strongly dependent on temperature at high temperature approaching those that produce thermionic-emission current. This tendency is characteristic for the current in Eq. (2). At low temperature, temperature dependence is determined in accordance with tunneling. At temperature high enough to create electrons that have higher energy than SBH, reverse current follows thermally activated types of temperature dependence. It is therefore concluded that some mechanisms increase tunneling current in the Ni and Mo SBDs but not in the Ti SBD.

Since tunneling current depends on SBH, barrier thickness, and electron mass, the large difference between the measured reverse currents of the Ni and Mo SBDs and the calculated ones is considered hereafter from viewpoints of low barrier patch,[19,20] GD,[21,22] thin surface barrier,[23,24] and electron effective mass.[25,26] Note that a surface pit on SiC is reported to cause high reverse current, since it enhances the electric field.[32,33] This mechanism does not apply to the case of the fabricated Ni and Mo SBDs, since the surface pit should also exist on the Ti SBD. In addition, the surface pit should alter the dependences of reverse current on electric field,[33] which is not the case for the fabricated SBDs, which show similar dependences on electric field, as shown in Fig. 8. In a similar analogy, trap-assisted tunneling, which also increases tunneling current, does not cause the high reverse current of the fabricated Ni and Mo SBDs. Since trap-assisted tunneling is a two-or-more-step process, it shows weaker dependences on electric field than on tunneling current of the one-step process expressed in Eq. (2).[34]

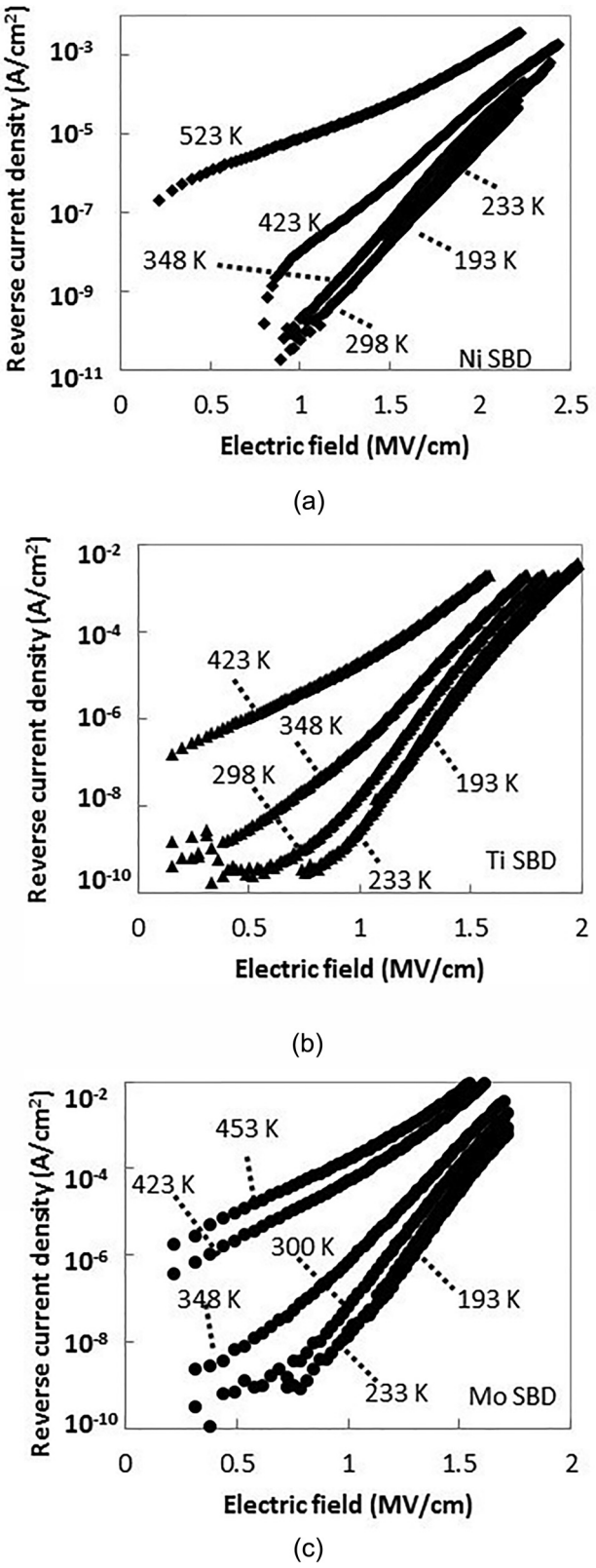


FIG. 7. Reverse characteristics of (a) Ni, (b) Ti, and (c) Mo SBDs at various temperatures.

## IV. DISCUSSION

### A. Low-barrier patch

The measured high reverse currents of SiC SBDs were explained by Zheng *et al*. and Furno *et al*. by assuming inhomogeneous SBH.[35,36] One approach to address the inhomogeneous SBH is to assume an embedded low-barrier region in the homogeneous high-barrier region. Inhomogeneity in SBH of SiC SBDs in forward characteristics has been reported.[37–40] If the area of the low-barrier region is large, the forward *I-V* characteristic shows a hump,[41] which is not the case for the fabricated SBDs, as shown in Fig. 4. On the

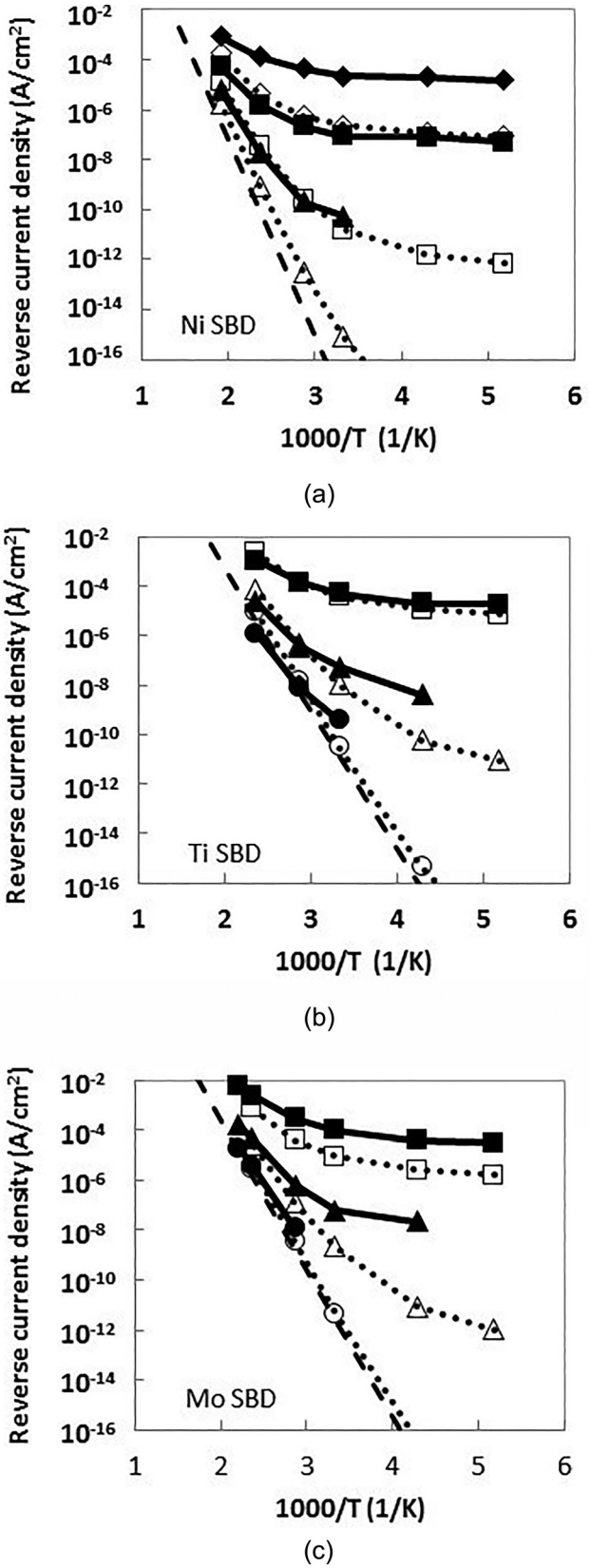


FIG. 8. Temperature dependences of reverse current density for (a) Ni, (b) Ti, and (c) Mo SBDs. Filled symbols represent measured values, and open symbols represent values calculated from Eq. (2) with a Schottky barrier height of 1.6 eV for Ni and 1.2 eV for Ti. The effective mass of 0.25 $m_0$ was used in the calculation. Electric fields at the Schottky interface are 0.6 (circle), 1.0 (triangle), 1.5 (square), and 2.0 MV/cm (diamond). Dashed lines show thermionic emission currents at 1.0 MV/cm.

other hand, if the area of the low-barrier region is within the extent of the potential of the surrounding high-SBH region, the forward *I-V* characteristic does not show a hump. This type of low-barrier region is called a "low-barrier patch."[19,20,37–40] In the presence of the low-barrier patch, an anomaly in the forward *I-V* characteristic can be observed at low temperature, since the proportion of the current flowing through the low-barrier patch becomes large at low temperature. Accordingly, the influence of the low-barrier patch in regard to the fabricated SBDs was examined.

Forward I-V characteristics of the Ni, Ti, and Mo SBDs at various temperatures fitted with Eq. (1a) are shown in Figs. 9(a)–9(c). Parameters extracted from Figs. 9(a)–9(c) are listed in Table I. Temperature dependences of ideality factor and SBH are plotted in Fig. 10. The ideality factor and SBH of the Ni, Ti, and Mo SBDs are weakly dependent on temperature. To extract the parameters of the low-barrier patch, $nk_BT$ is plotted against $k_BT$ in Figs. 11(a)–11(c), where $n$ is the ideality factor, $k_B$ is the Boltzmann's constant, and $T$ is the temperature. The $nk_BT$ vs. $k_BT$ plots of the Ni, Ti, and Mo SBDs are parallel to those of the ideal case of $n = 1$. By fitting the ideality factor with the equation $n = 1 + T_0/T$, $T_0$ values are obtained as 10.0, 6.70, and 15.5 K for the Ni, Ti, and Mo SBDs, respectively. Under the assumption that the low-barrier patch is circular, the potential of the center of the patch is the lowest. Since the potential also distributes in the depth direction, the saddle point in the potential distribution appears at some depth into SiC from the Schottky interface. When the distribution of SBHs of the low-barrier patches is Gaussian, the average potential of the saddle point, $\phi_B^{sad}$, is expressed as[19,20]

$$\phi_B - \phi_B^{sad} = \sigma\left(\frac{\sqrt{2}V_i}{z_{dep}}\right)^{2/3}, \tag{4a}$$

$$\frac{k_BT_0}{q} = \frac{\sigma^2}{3}\left(\frac{qN_D}{\varepsilon_r\varepsilon_0\sqrt{V_i}}\right)^{2/3}, \tag{4b}$$

where $\phi_B$ is SBH in the normal area, $\sigma$ the patch parameter, $V_i$ potential difference between the conduction band at the Schottky interface and that in the bulk, $z_{dep}$ width of the depletion layer, $N_D$ donor density, and $\varepsilon_r$ the relative dielectric constant. Barrier lowering induced by the low-barrier patch at 298 K, i.e., $\phi_B - \phi_B^{sad}$, is 0.060, 0.041, and 0.064 eV for the Ni, Ti, and Mo SBDs, respectively. $\sigma$ of 6.26, 4.76, and $8.12 \times 10^{-5}$ $V^{1/3}$ $cm^{2/3}$ and $V_i$ of 0.220, 0.219, and 0.228 V were used to calculate $\phi_B - \phi_B^{sad}$ for the Ni, Ti, and Mo SBDs, respectively. Since all SBDs show similar barrier lowering and these amounts of barrier lowering cannot explain the high reverse current of the Ni and Mo SBDs shown in Fig. 6, it is concluded that the low-barrier patch is not the cause of the high reverse currents of the Ni and Mo SBDs.

### B. Gaussian distribution of barrier height

Another approach to handle inhomogeneous SBH is to assume that SBH has a Gaussian distribution (GD).[21,22] The parameters of the GD can be extracted from the temperature

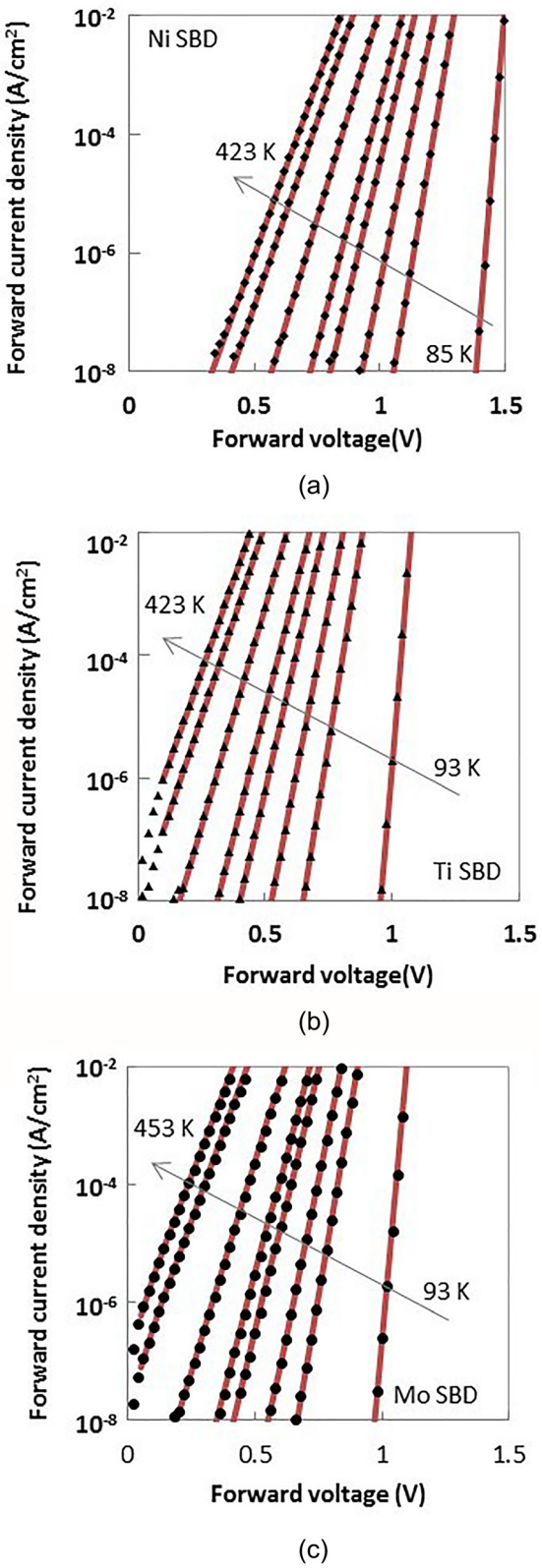


FIG. 9. Forward characteristics of (a) Ni, (b) Ti, and (c) Mo SBDs at various temperatures fitted with the thermionic-emission theory expressed as Eq. (1). Temperatures are listed in Table I.

dependence of forward *I-V* characteristics shown in Fig. 9. Under the GD assumption, SBH extracted from $J_s$ in Eq. (1) is called "apparent barrier height" ($\phi_{ap}$), which is expressed as[21,22]

TABLE I. Parameters extracted from forward characteristics of Ni, Ti, and Mo SBDs by using Eq. (1a).

| Temperature (K) | Ideality factor (n) | $\phi_B$ (eV) | $J_s$ (A/cm$^2$) |
|---|---|---|---|
| Ni SBD | | | |
| 85 | 1.11 | 1.49 | $8.53 \times 10^{-83}$ |
| 193 | 1.04 | 1.57 | $4.88 \times 10^{-35}$ |
| 233 | 1.04 | 1.58 | $5.10 \times 10^{-28}$ |
| 273 | 1.03 | 1.59 | $4.86 \times 10^{-23}$ |
| 298 | 1.03 | 1.60 | $1.36 \times 10^{-20}$ |
| 348 | 1.02 | 1.61 | $9.18 \times 10^{-17}$ |
| 398 | 1.02 | 1.62 | $8.00 \times 10^{-14}$ |
| 423 | 1.02 | 1.62 | $1.29 \times 10^{-12}$ |
| Ti SBD | | | |
| 93 | 1.07 | 1.15 | $4.21 \times 10^{-57}$ |
| 193 | 1.03 | 1.20 | $2.93 \times 10^{-25}$ |
| 233 | 1.03 | 1.20 | $8.75 \times 10^{-20}$ |
| 273 | 1.02 | 1.21 | $6.17 \times 10^{-16}$ |
| 298 | 1.03 | 1.20 | $8.05 \times 10^{-14}$ |
| 348 | 1.02 | 1.21 | $5.16 \times 10^{-11}$ |
| 398 | 1.02 | 1.22 | $8.15 \times 10^{-9}$ |
| 423 | 1.01 | 1.23 | $6.65 \times 10^{-8}$ |
| Mo SBD | | | |
| 93 | 1.15 | 1.11 | $1.64 \times 10^{-54}$ |
| 193 | 1.05 | 1.20 | $2.80 \times 10^{-25}$ |
| 233 | 1.03 | 1.23 | $2.55 \times 10^{-20}$ |
| 273 | 1.03 | 1.22 | $3.04 \times 10^{-16}$ |
| 298 | 1.03 | 1.23 | $1.73 \times 10^{-14}$ |
| 348 | 1.03 | 1.24 | $1.98 \times 10^{-11}$ |
| 423 | 1.01 | 1.26 | $2.66 \times 10^{-8}$ |
| 453 | 1.00 | 1.27 | $2.34 \times 10^{-7}$ |

$$\phi_{ap} = \bar{\phi}_{b0} - \frac{\sigma_0^2 q}{2k_B T}, \tag{5}$$

where $\bar{\phi}_{b0}$ is the mean barrier height at zero bias, and $\sigma_0$ is the standard deviation of barrier height at zero bias. Here, the linear bias dependence such as $\bar{\phi}_b = \bar{\phi}_{b0} + \gamma V_F$, $\sigma = \sigma_0 + \xi V_F$, is assumed.[21] The coefficients are related to ideality factor ($n$) in Eq. (1a), which is also called apparent ideality factor ($n_{ap}$) in the GD scheme, as

$$\frac{1}{n_{ap}} = (1-\gamma) + \frac{\sigma_0 q \xi}{k_B T}. \tag{6}$$

Dependences of $\phi_{ap}$ on inverse temperature are shown in Fig. 12. $\bar{\phi}$ b0 and $\sigma_0$ are extracted as 1.646, 1.235, 1.298 eV and 0.049, 0.036, 0.056 V for Ni, Ti, and Mo SBDs, respectively. Dependence of $1/n_{ap}$ on the inverse temperature is shown in Fig. 13. The coefficients of bias dependence, $\gamma$ and $\xi$, are extracted as −0.00083, 0.0010, −0.025 and −0.015, −0.015, −0.022 for Ni, Ti, and Mo SBDs, respectively. Since the differences between $\sigma_0$, $\gamma$, and $\xi$ for the fabricated SBDs are small, the GD of barrier height cannot explain the high reverse currents of the Ni and Mo SBDs.

The activation-energy equation is investigated next. The Richardson plot is modified under the GD assumption as[21,22]

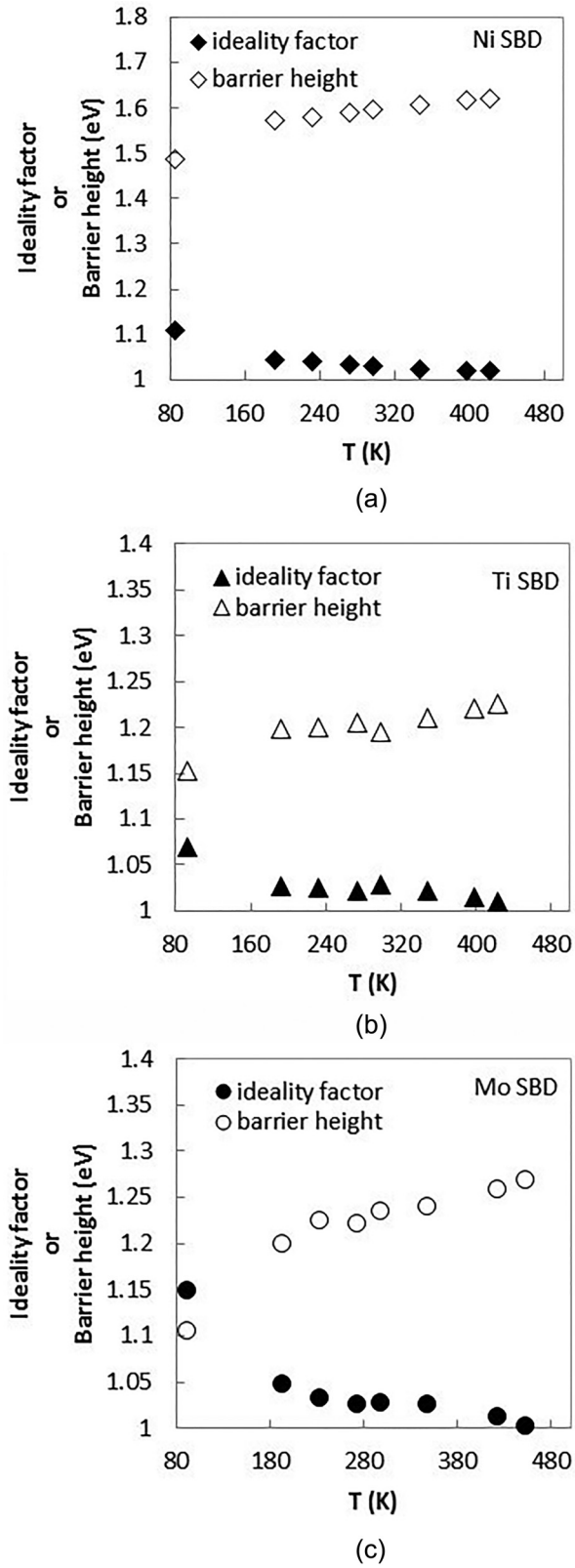


FIG. 10. Temperature dependences of ideality factor (filled symbols) and Schottky barrier height (open symbols) for the (a) Ni, (b) Ti, and (c) Mo SBDs.

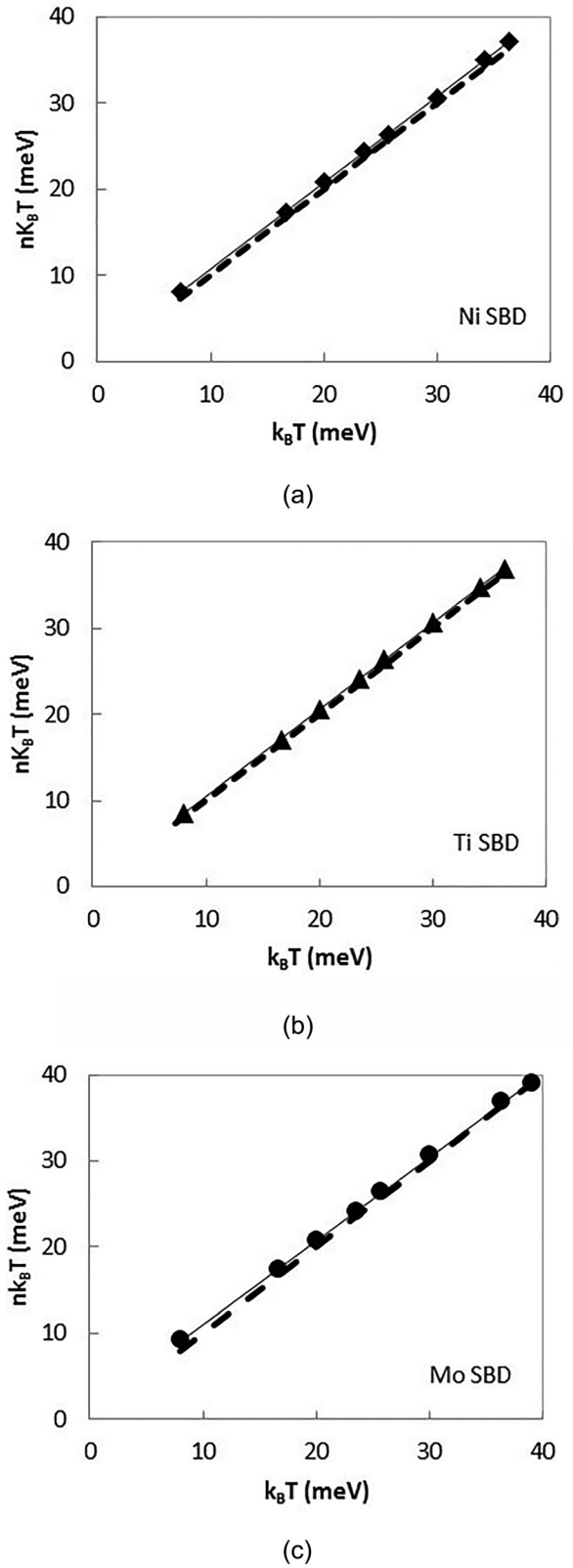


FIG. 11. $nk_BT$ vs. $k_BT$ plots for the (a) Ni, (b) Ti, and (c) Mo SBDs fitted with $n = 1 + T_0/T$. Dashed line represents the ideal case, i.e., $n = 1$.

$$\ln\left(\frac{J_s}{T^2}\right) - \frac{q^2\sigma_0^2}{2k_B^2T^2} = \ln(A^{**}) - \frac{q\bar{\phi}_{b0}}{k_BT}. \quad (7)$$

Activation energy is plotted in Fig. 14, which gives $A^{**}$ and $\bar{\phi}$ b0 as 170, 159, and 169 A/cm$^2$ K$^2$ and 1.649, 1.236, and 1.301 eV for the Ni, Ti, and Mo SBDs, respectively. Note that the Richardson constant, $A^{**}$, extracted from Fig. 14 is different from the theoretical value of 146 A/cm$^2$K$^2$.[3] However, since $\phi_B$ in Eq. (1a) is not strongly dependent on $A^{**}$, the extraction of $\phi_B$ using theoretical $A^{**}$ is

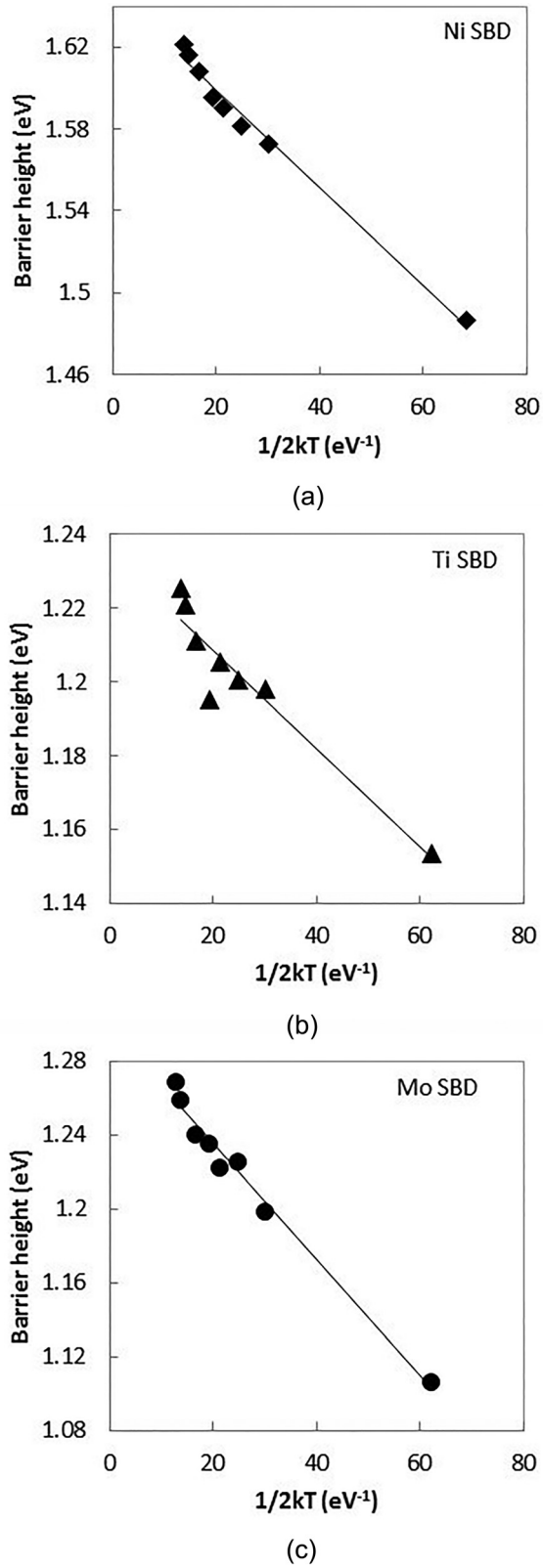


FIG. 12. Barrier height vs. 1/2*kT* plots for the (a) Ni, (b) Ti, and (c) Mo SBDs.

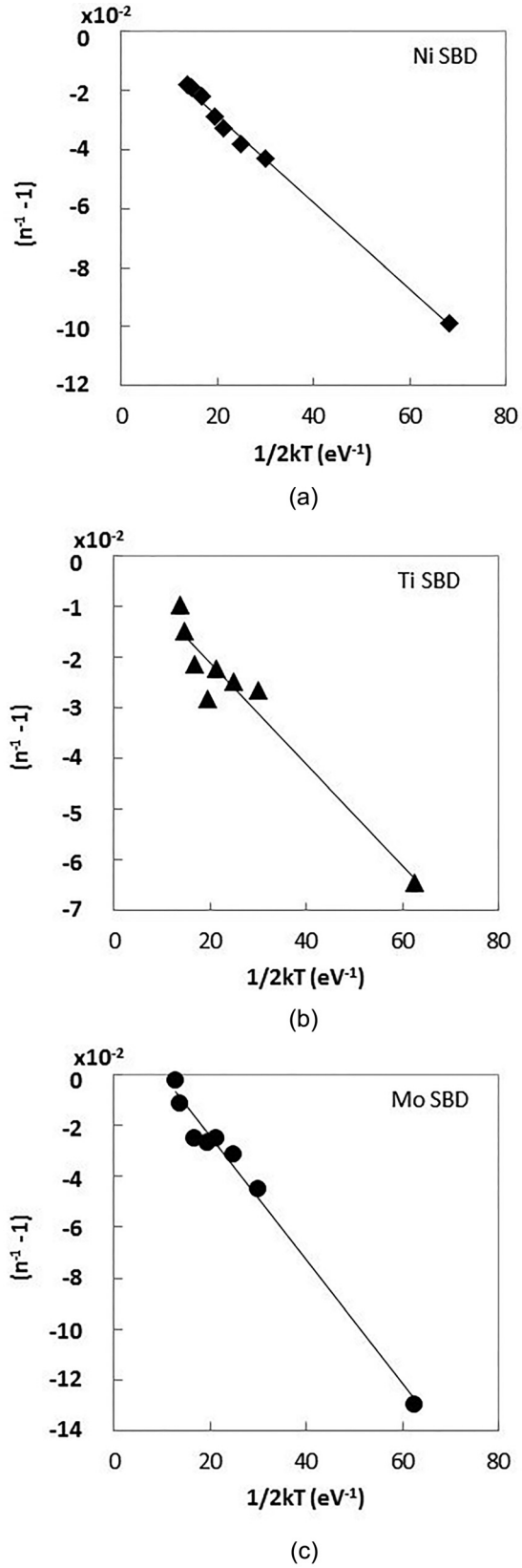


FIG. 13. Ideality factor vs. 1/2*kT* plots for the (a) Ni, (b) Ti, and (c) Mo SBDs.

reasonable. This result is validated from the fact that $\bar{\phi}$ b0 extracted from Fig. 12 is similar to $\bar{\phi}$ b0 extracted from Fig. 14. Extracted $A^{**}$ is recalled in the section on effective mass.

### C. Thin surface barrier

In some studies of GaN SBDs,[23,24] high leakage current is explained by high impurity concentration at the Schottky interface, since the Schottky barrier becomes thin, as shown

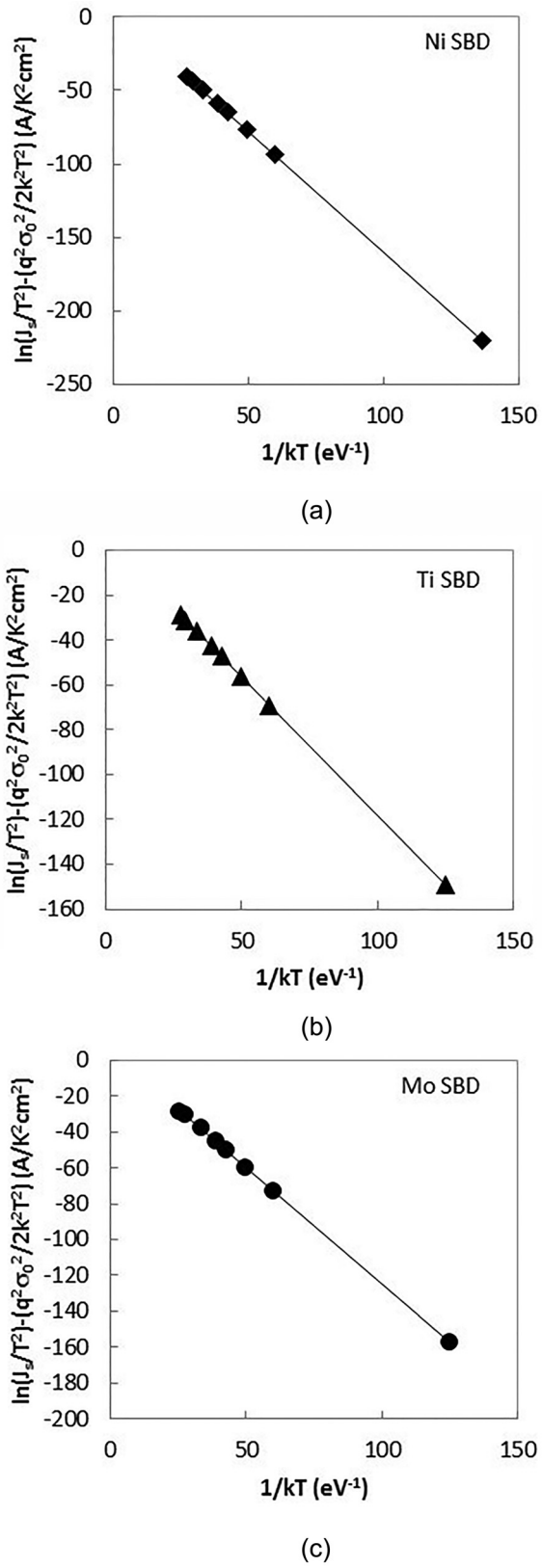


FIG. 14. Modified Richardson plots for the (a) Ni, (b) Ti, and (c) Mo SBDs.

in Fig. 15, and tunneling current thereby increases. This type of interface is called a thin surface barrier, and a nitrogen vacancy is proposed as the origin of high impurity concentration of a GaN SBD.[23,24] Whether the same mechanism can

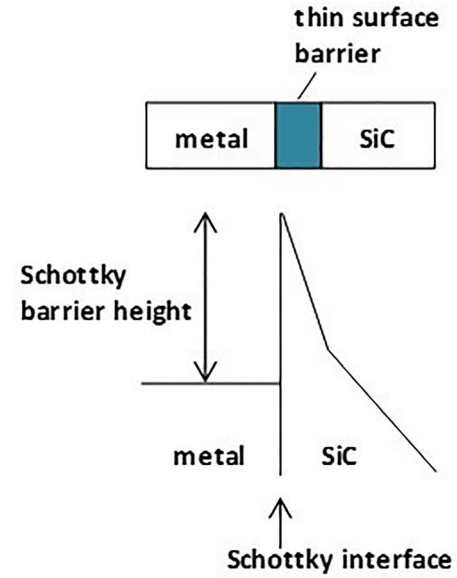


FIG. 15. (Top) Schematic view around thin surface barrier and (bottom) potential distribution in the presence of thin surface barrier.

be applied to explain the high reverse current of our Ni and Mo SiC-SBDs is examined below.

Measured reverse current of the Ni SBD and that calculated from Eq. (2) in the presence of a homogeneous thin surface barrier with the thickness of 5 nm and impurity concentration of 1e19 $cm^{-3}$ are plotted in Fig. 16. Since the thin surface barrier is characterized by both its thickness and impurity concentration, the combination of the above-stated thickness and impurity concentration is not unique, but they are the typical values that reproduce measured reverse current. Thus, a thinner surface barrier with a higher impurity concentration or a thicker surface barrier with a lower impurity concentration can also fit the measured values.

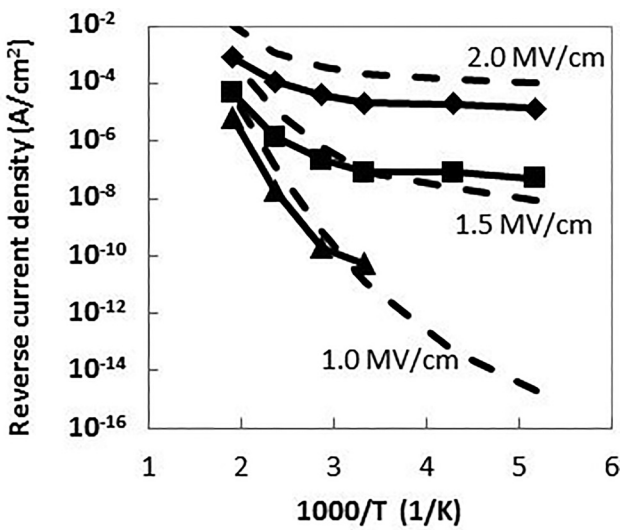


FIG. 16. Temperature dependences of the measured reverse current of the Ni SBD (solid lines with filled symbols) and tunneling current calculated from Eq. (2) in the presence of a thin surface barrier (dashed lines). The impurity concentration and the thickness of the barrier are $1 \times 10^{19}$ $cm^{-3}$ and 5 nm, respectively. The calculation was performed with SBH of 1.60 eV and the effective mass of 0.25 $m_0$. The electric field mentioned in the figure is the electric field at the bottom of the thin surface barrier.

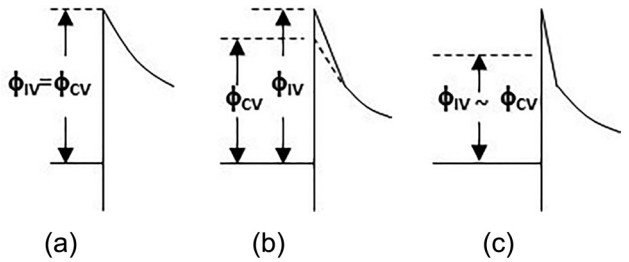


FIG. 17. Schematics of potential distribution near the Schottky interface with SBH extracted from C-V characteristics ($\phi_{CV}$) and forward I-V characteristics ($\phi_{IV}$). (a) Ideal state, where $\phi_{CV}$ equals $\phi_{IV}$. (b) The potential distribution with moderate thin surface barrier, where $\phi_{CV}$ is lower than $\phi_{IV}$. (c) Potential distribution with the thin surface barrier, where electrons can tunnel in the forward state, and $\phi_{IV}$ is smaller than the ideal SBH.

The existence of the thin surface barrier was verified by measuring *C-V* characteristics. Potential distributions near the Schottky interface with SBH extracted from *C-V* characteristics ($\phi_{CV}$) and forward *I-V* characteristics ($\phi_{IV}$) are schematically illustrated in Figs. 17(a)–17(c). In the ideal state [Fig. 17(a)], $\phi_{CV}$ equals $\phi_{IV}$. In the presence of a moderately thin surface barrier [Fig. 17(b)], $\phi_{CV}$ is lower than $\phi_{IV}$. If the surface barrier is very thin, as shown in Fig. 17(c), electrons can tunnel in the forward state, and $\phi_{IV}$ becomes smaller than the ideal SBH.[42] In this case, $\phi_{CV}$ is similar to $\phi_{IV}$, and tunneling current calculated from Eq. (2) with $\phi_{IV}$ is smaller than the actual reverse current.

The *C-V* characteristic of the Ni SBD at 298 K is shown in Fig. 18. SBH is extracted from the intersection with the x-axis as 1.69 eV, which is higher than $\phi_{IV}$ of 1.60 eV. This result indicates that the thin surface barrier does not cause the high reverse current of the Ni SBD. And $\phi_{CV}$ obtained from the thin surface barrier with the thickness of 5 nm and impurity concentration of 1e19 $cm^{-3}$ should be 0.24 eV lower than the ideal SBH. Note that $\phi_{CV}$ is an average value over the whole interface. Thus, if a local thin surface barrier exists, it cannot be detected from the *C-V* characteristic.

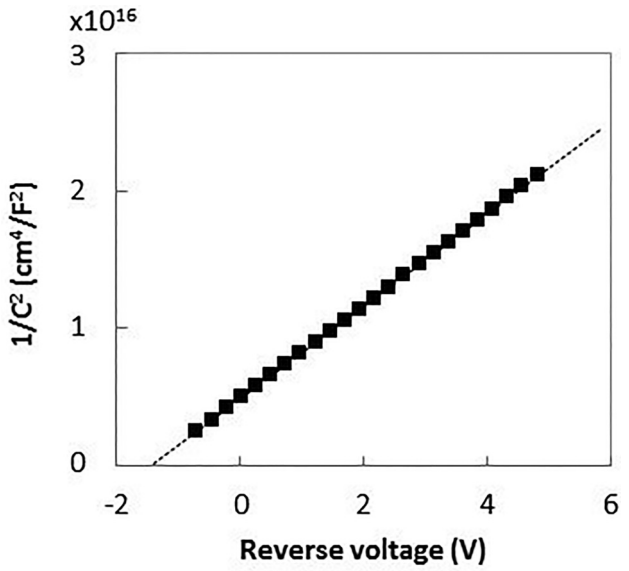


FIG. 18. Measured *C-V* characteristic of the Ni SBD.

However, the local thin surface barrier could affect the forward *I-V* characteristic in a similar way to the low-barrier patch. As described in the section on the low barrier patch, it is concluded that the local thin surface barrier is not the cause of the high reverse current of the Ni SBD either.

The Mo SBD was also investigated under the same assumption. Measured reverse current of the Mo SBD and the calculated one using Eq. (2) in the presence of a homogeneous thin surface barrier with the thickness of 5 nm and impurity concentration of 3.5e18 $cm^{-3}$ are plotted in Fig. 19. The *C-V* characteristic of the Mo SBD at 298 K is shown in Fig. 20. SBH is extracted from the intersection with the x-axis as 1.38 eV, which is higher than $\phi_{IV}$ of 1.23 eV. This result indicates that the thin surface barrier is not the cause of the high reverse current of the Mo SBD (as is the case for the Ni SBD).

### D. Effective mass

To simplify the calculation, in Eq. (2), the same electron effective mass was used for metals and SiC. In particular, whether the difference in the effective masses of metals and SiC can explain the measured high reverse current of the Ni and Mo SBDs was examined as follows. The influence of effective mass on tunneling current was studied in regard to a $Si/SiO_2$ system,[25,26] and the same procedure as described in the literatures was followed. In the case of one-step elastic tunneling, total electron energy and the wave number parallel to the Schottky interface are conserved. When the effective mass of electrons in a metal is different from that of electrons in SiC, the electron energy perpendicular to the Schottky interface is not conserved and is expressed as[25,26]

$$E_{sl} = E_{ml} + E_{mt} - E_{st}, \tag{8a}$$

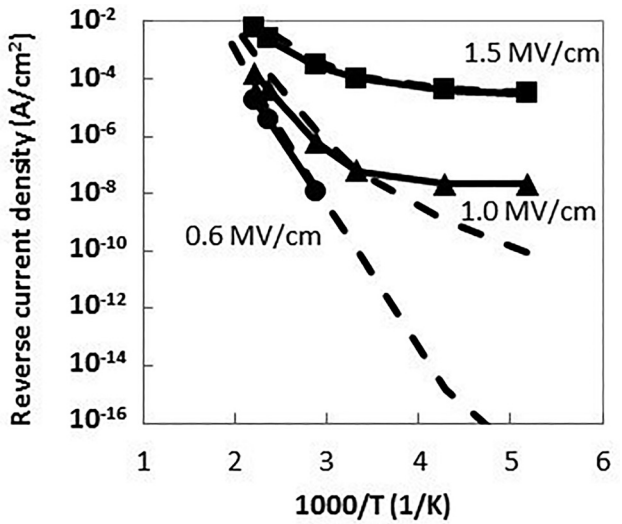


FIG. 19. Temperature dependences of measured reverse current of the Mo SBD (solid lines with filled symbols) and tunneling current calculated from Eq. (2) in the presence of a thin surface barrier (dashed lines). The impurity concentration and the thickness of the barrier are $3.5 \times 10^{18}$ $cm^{-3}$ and 5 nm, respectively. The calculation was performed with SBH of 1.23 eV and the effective mass of 0.25 $m_0$. The electric field mentioned in the figure is the electric field at the bottom of the thin surface barrier.

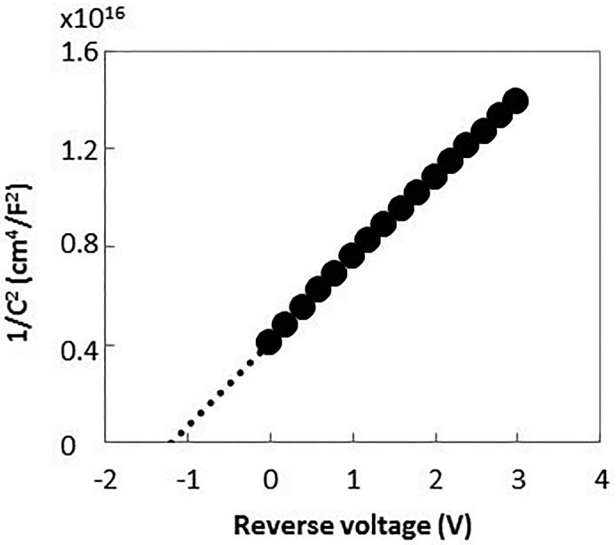


FIG. 20. Measured *C-V* characteristic of the Mo SBD.

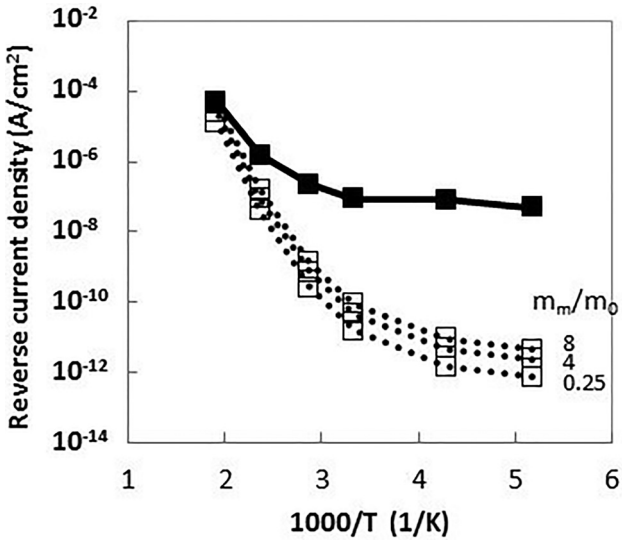


FIG. 21. Temperature dependences of tunneling current calculated from Eq. (9) and measured reverse current of the Ni SBD. Filled symbols represent measured currents of the Ni SBD. Open symbols represent calculated currents with SBH of 1.6 eV and the effective mass in SiC of 0.25 $m_0$. Effective masses for the metal are 0.25, 4, and 8 $m_0$. The electric field at the Schottky interface is 1.5 MV/cm.

$$= E_{\mathrm{ml}} + E_{\mathrm{mt}}\left(1 - \frac{m_{\mathrm{m}}}{m_{\mathrm{s}}}\right), \tag{8b}$$

where $E_{\mathrm{sl}}$ and $E_{\mathrm{st}}$ are, respectively, electron energies in SiC perpendicular and parallel to the Schottky interface, $E_{\mathrm{ml}}$ and $E_{\mathrm{mt}}$ are, respectively, electron energies in the metal perpendicular and parallel to the Schottky interface, $m_{\mathrm{m}}$ and $m_{\mathrm{s}}$ are, respectively, electron effective masses in the metal and SiC. Here, the isotropic effective mass and a parabolic relationship between energy and wave number, $E=\hbar^2k^2/2m$, are assumed. Tunneling current and tunneling probability are expressed as[25]

$$J = \frac{4\pi q m_{\mathrm{m}}}{h^3}\int_0^{\infty}\int T(E_{\mathrm{ml}}, E_{\mathrm{mt}}) f_{\mathrm{m}}(E_{\mathrm{ml}} + E_{\mathrm{mt}})\mathrm{d}E_{\mathrm{ml}}\mathrm{d}E_{\mathrm{mt}}, \tag{9a}$$

$$T(E_{\mathrm{ml}}, E_{\mathrm{mt}}) \sim \exp\left[-2\frac{\sqrt{2m_{\mathrm{s}}}}{\hbar} \times \int_{z_1}^{z_2}\sqrt{\phi(z) - E_{\mathrm{ml}} - E_{\mathrm{mt}}\left(1 - \frac{m_{\mathrm{m}}}{m_{\mathrm{s}}}\right)}\mathrm{d}z\right]. \tag{9b}$$

The occupation probability of electrons in SiC and the coefficient of tunneling probability were approximated as 0 and 1, respectively. Influence of the difference in effective masses on tunneling current was evaluated by using Eqs. (9). Calculated temperature dependences of tunneling current at electric field at the Schottky interface of 1.5 MV/cm are plotted with the measured reverse current of the Ni SBD in Fig. 21. The dependence of the tunneling current on $m^*$ in metal is clearly weak. This is because as $m^*$ increases, the coefficient of tunneling current increases, but the tunneling probability decreases. Cyclotron effective mass in the case of Ni is reported to be 8–8.8 $m_0$ at most,[43,44] but this large difference in $m^*$ for Ni and SiC cannot explain the high reverse current of the Ni SBD. The effective mass in the case of Mo is unknown, but the effective mass can be estimated from the electronic specific heat,[45] and the estimated mass is approximately 2 $m_0$, which also cannot explain the high reverse current of the Mo SBD.

Influence of $m^*$ in the case of SiC on tunneling current was investigated as follows. Since the difference in $m^*$ for metals and SiC has little influence on tunneling current, the same $m^*$ is assumed for metals and SiC for simplicity, and Eq. (2) is used to calculate tunneling current. Temperature dependences of calculated tunneling current for various $m^*$ and measured reverse current of the Ni SBD at an electric field at the Schottky interface of 1.5 MV/cm are plotted in Fig. 22. The measured reverse current of the Ni SBD is well explained by tunneling current for $m^*$ of 0.15 $m_0$, whereas that of the Ti SBD is well explained by the tunneling current for $m^*$ of 0.25 $m_0$, as mentioned before. Measured reverse current of the Ni SBD and calculated tunneling current for $m^*$ of 0.15 $m_0$ are compared for other electric fields in Fig. 23, in which they show good agreement. The case for the Mo SBD, in which tunneling current calculated with $m^*$ of 0.20 $m_0$ reproduces measured reverse current, is shown in Fig. 24. According to these results, the effective mass near the Schottky interface in SiC is possibly dependent on metal species.

Since the lattice deformation in SiC is reported to change effective mass,[46] Schottky interfaces were investigated. Transmission electron diffraction (TED) patterns obtained for Ni, Ti, Mo, and SiC are shown in Fig. 25. The patterns for SiC are similar irrespective of the metal species on SiC. The electron beam (with spot size of 1 nm) was injected 15 nm from the Schottky interfaces. Although the crystal structures that can be investigated by TED are local structures, similar diffraction patterns to those shown in Fig. 25 from another site in metals were obtained. From the diffraction patterns, the crystal structures of Ti and SiC were determined to be hexagonal close packed (hcp), that of Ni to be face-centered cubic (fcc), and that of Mo to be

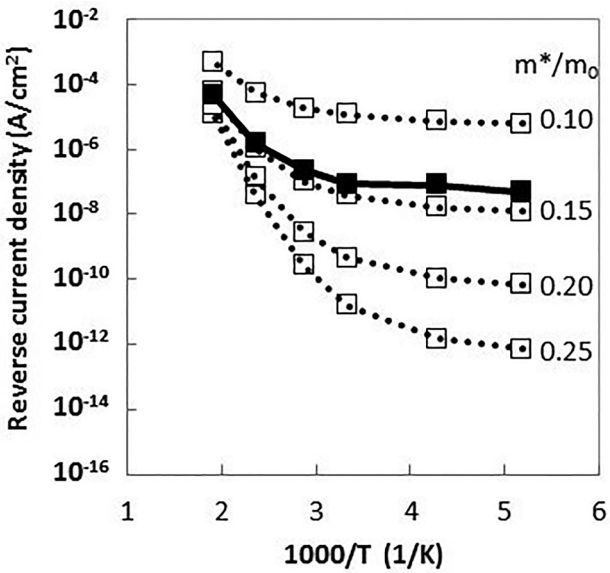


FIG. 22. Temperature dependences of the calculated tunneling current for various $m^*$ and measured reverse current of the Ni SBD at the electric field at the Schottky interface of 1.5 MV/cm. Filled symbols represent measured currents of the Ni SBD. Open symbols represent currents calculated from Eq. (2) with SBH of 1.6 eV and effective masses of 0.10, 0.15, 0.20, and 0.25 $m_0$.

body-centered cubic (bcc). The crystallographic relationships near the Schottky interfaces were determined as

$$(0001)_{\mathrm{Ti}}||(0001)_{\mathrm{SiC}}, [1-100]_{\mathrm{Ti}}||[1-100]_{\mathrm{SiC}},$$
$$(11-1)_{\mathrm{Ni}}||(0001)_{\mathrm{SiC}}, [112]_{\mathrm{Ni}}||[1-100]_{\mathrm{SiC}},$$
$$(110)_{\mathrm{Mo}}||(0001)_{\mathrm{SiC}}, [1-10]_{\mathrm{Mo}}||[1-100]_{\mathrm{SiC}}.$$

Note that the crystallographic relationships are not universal, and different relationships, which might depend on fabrication conditions, have been reported.[47,48] The inter-atomic

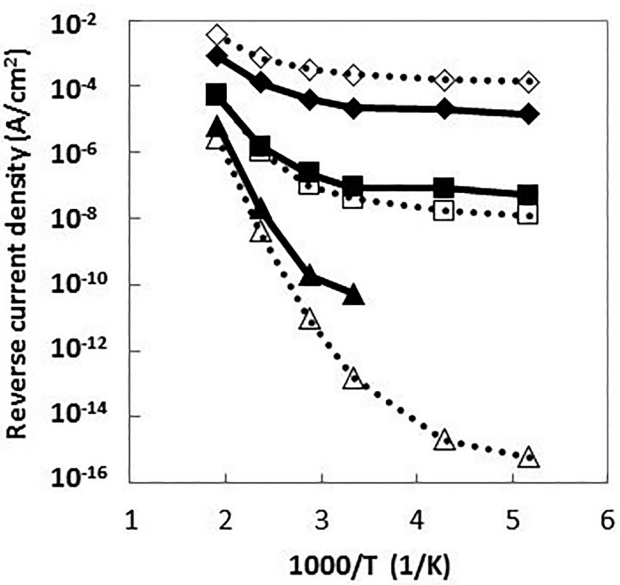


FIG. 23. Temperature dependence of reverse current. Filled symbols represent measured currents of the Ni SBD. Open symbols represent currents calculated from Eq. (2) with SBH of 1.60 eV and the effective mass of 0.15 $m_0$. Electric fields at the Schottky interface are 1.0 (triangle), 1.5 (square), and 2.0 MV/cm (diamond).

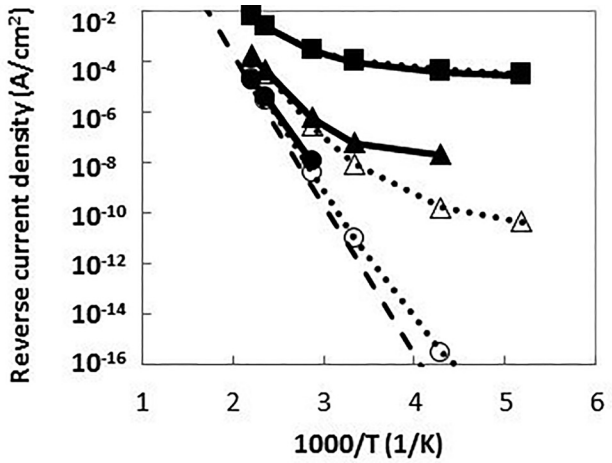


FIG. 24. Temperature dependences of reverse current. Filled symbols represent measured currents of the Mo SBD. Open symbols represent calculated currents using Eq. (2) with SBH of 1.23 eV and effective mass of 0.20 $m_0$. The electric field at the Schottky interface is 0.6 (circle), 1.0 (triangle), and 1.5 MV/cm (square).

distance in metals and its deviation from the substrate (4H-SiC) are listed in Table II. They were calculated by using the above-stated crystallographic relationships and the lattice constant of Ti of a = 0.295 nm,[49] Ni of a = 0.249 nm,[50] SiC of a = 0.307 nm,[51] and Mo of a = 0.315 nm[52] under the assumption that crystallographic relationships are preserved at the Schottky interfaces. As for the Ti SBD, a small lattice mismatch exists. On the other hand, the Mo SBD shows a large lattice mismatch in the $[1\text{–}100]_{\mathrm{SiC}}$ direction, and the Ni SBD shows a large lattice mismatch in both the $[11\text{–}20]_{\mathrm{SiC}}$ and $[1\text{–}100]_{\mathrm{SiC}}$ directions.

As shown in Fig. 6, the extent of the deviation between measured reverse current and calculated tunneling current is

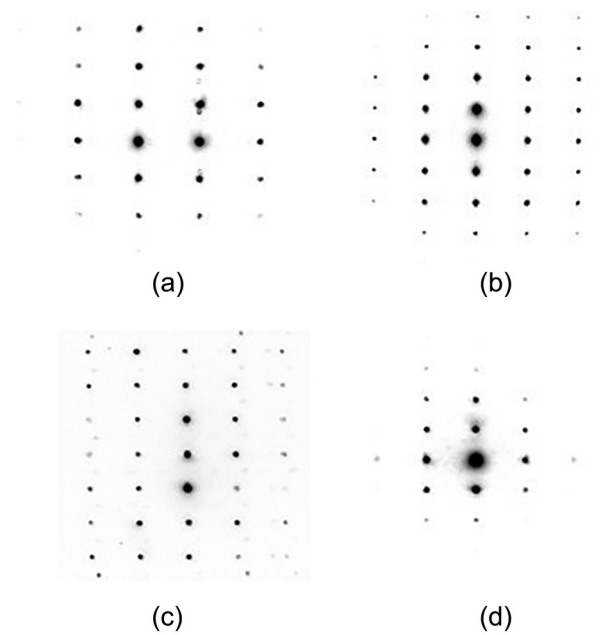


FIG. 25. TED patterns from (a) Ni, (b) Ti, (c) Mo, and (d) SiC of SBDs (colors reversed). Electrons (with an acceleration voltage of 200 kV) were injected in the $[1\text{–}100]_{\text{4H-SiC}}$ direction at 15 nm distant from the Schottky. The patterns from SiC are the same irrespective of the metal species on SiC.

TABLE II. Inter-atomic distances for Ti, Ni, and Mo on 4H-SiC(0001), and lattice mismatch between metals and SiC.

| | | Ti (hcp) | Ni (fcc) | Mo (bcc) |
|---|---|---|---|---|
| $[1\text{-}100]_{SiC}$ | Inter-atomic distance (nm) | 0.511 | 0.431 | 0.444 |
| | Mismatch (%) | −4.17 | −23.5 | −19.9 |
| $[11\text{-}20]_{SiC}$ | Inter-atomic distance (nm) | 0.295 | 0.249 | 0.314 |
| | Mismatch (%) | −4.17 | −23.5 | 2.13 |

large for the Ni SBD, moderately large for the Mo SBD, and very small for the Ti SBD. This tendency is qualitatively similar to that of the extent of lattice mismatch (Table II). Since the large lattice mismatch of the Mo and Ni SBDs is thought to generate transition layers at the Schottky interfaces, the Schottky interface was observed precisely by the transmission electron microscopy (see TEM images in Fig. 26). As for the Ti SBD, a smooth transition from SiC to Ti is observed at the Ti-SiC boundary. On the other hand, the metal-SiC boundaries of the Ni and Mo SBDs are not smooth, probably due to transition layers. The transition layers are thought to be formed by the deformation of SiC from the bulk. Since the transition layers possess band structures that differ from that of bulk SiC, due to different crystal structures, they represent a different effective mass from that of bulk SiC.[46] Although it is still being debated whether or not effective mass can be as small as 0.15 $m_0$, the result of the present study indicates that not only work function but also lattice constant is important in regard to selecting the metal species as the Schottky metal for wide band-gap SBDs (in the case of which tunneling current dominates reverse current). The possibility of silicide formation is briefly discussed as follows. The annealing temperature after metal deposition in the case of the fabricated Ni SBD is lower than the temperature of silicide formation. Nickel silicide is reported to form on the Si-face of 4H-SiC at 873 K, but not at 673 K.[47] It is thus concluded that silicide formation is not possible in the case of the fabricated Ni SBD. Titanium carbide and Mo silicide are not thought to be formed in the case of the fabricated SBDs, either. Titanium carbide is reported to be formed at 773 K.[53,54] And Mo is expected to show a higher reaction temperature, since it is a refractory metal.

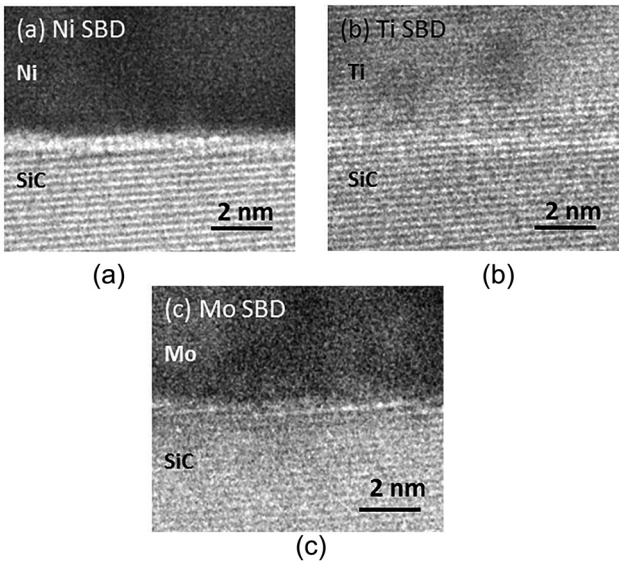


FIG. 26. TEM images of (a) the Ni, (b) Ti, and (c) Mo SBDs near the Schottky interface. Electrons (with an acceleration voltage of 300 kV) were injected in the $[1\text{–}100]_{4H\text{-}SiC}$ direction.

Effective mass concerning forward characteristics and that concerning reverse characteristics for SiC SBDs are briefly discussed as follows. Since the Richardson constant, $A^{**}$, in Eq. (1) is a function of effective mass, the effective mass can be deduced from the forward characteristics in Fig. 14 as 0.245, 0.228, and 0.243 for Ni, Ti, and Mo SBDs, respectively. The effective mass concerning forward characteristics, $m^*_F$, when constant-energy surfaces are ellipsoids, is expressed as[55]

$$m^*_F = \sqrt{l_1 m_2 m_3 + l_2 m_3 m_1 + l_3 m_1 m_2}, \tag{10}$$

where $l_i$ is the direction cosine of the normal to the Schottky interface relative to the principal axis of the ellipsoid, and $m_i$ is the component of the effective mass tensor. For the SBDs fabricated in this study, $m^*_F$ is $\sqrt{m_{M\Gamma} m_{MX}}$, where the notation of symmetry points in the Brillouin zone follows that given in the literature (for example, $M\Gamma$ and $MX$ are parallel to the $(0001)_{SiC}$ surface).[30] On the other hand, the effective mass concerning the reverse characteristics in Eq. (3), i.e., $m^*_R$, is $m_{ML}$, where ML is perpendicular to the $(0001)_{SiC}$ surface. Thus, $m^*_F$ and $m^*_R$ are different. Furthermore, $m^*_R$ does not represent the effective mass in the bulk of a metal or a semiconductor; instead, it represents the effective mass in the tunneling region, as shown in Fig. 1(b). In the case of the developed SBDs, $m^*_R$ represents the effective mass near the Schottky interface with the thickness of several nanometers, whose structure can be altered from that of the bulk, as shown in Fig. 26. Although $m^*_F$ is also affected by the Schottky potential barrier, $m^*_R$ is more sensitive to the interface structure because the potential is steeper due to the high reverse electric field. Therefore, the effective mass extracted from the forward characteristics does not contradict that deduced from the reverse characteristics.

## V. CONCLUSIONS

Reverse currents of Ni, Ti, and Mo/SiC SBDs were investigated from the viewpoints of temperature dependence, low barrier patch, GD, thin surface barrier, and electron effective mass. The temperature dependence of reverse current shows a tunneling-like behavior; that is, it is weak at low temperature but strong at high temperature. Measured reverse current of the Ti SBD is well reproduced by the tunneling current in the case of an effective mass of 0.25 $m_0$, whereas those of the Ni and Mo SBDs are higher than the tunneling current in the case of an effective mass of 0.25 $m_0$. The high reverse currents cannot be explained in terms of low barrier patch, GD, or thin surface barrier; however, the measured reverse currents of the Ni and the Mo SBDs are well explained by the tunneling current in the cases of effective masses of 0.15 and 0.20 $m_0$. The small effective mass is possibly attributable to the lattice mismatch between metals and SiC. The lattice constant as well as the work function is

important in selecting the metal species as the Schottky metal for wide band-gap SBDs, for which tunneling current dominates reverse current.

## ACKNOWLEDGMENTS

The authors thank Dr. M. Koguchi for his valuable discussions and critical comments.

[1]R. A. Wood and T. E. Salem, IEEE Trans. Power Electron. **26**, 2504 (2011).
[2]L. M. Porter and R. F. Davis, Mater. Sci. Eng. B **34**, 83 (1995).
[3]A. Itoh and H. Matsunami, Phys. Status Solidi A **162**, 389 (1997).
[4]O. Shigiltchoff, S. Bai, R. P. Devaty, W. J. Choyke, T. Kimoto, D. Hobgood, P. G. Neudeck, and L. M. Porter, Mater. Sci. Forum **433–436**, 705 (2003).
[5]T. Teraji and S. Hara, Phys. Rev. B **70**, 035312 (2004).
[6]F. Roccaforte, F. Giannazzo, and V. Raineri, J. Phys. D: Appl. Phys. **43**, 223001 (2010).
[7]S. M. Sze and K. K. Ng, *Physics of Semiconductor Devices*, 3rd ed. (New Jersey, Wiley, 2007).
[8]T. Hatakeyama and T. Shinohe, Mater. Sci. Forum **389-393**, 1169 (2002).
[9]H. Fujiwara, T. Kimoto, T. Tojo, and H. Matsunami, Appl. Phys. Lett. **87**, 051912 (2005).
[10]Y. Wang, G. N. Ali, M. K. Mikhov, V. Vaidyanathan, B. J. Skromme, B. Raghothamachar, and M. Dudley, J. Appl. Phys. **97**, 013540 (2005).
[11]A. Grekov, Q. Zhang, H. Fatima, A. Agarwal, and T. Sudarshan, Microelectron. Reliab. **48**, 1664 (2008).
[12]R. A. Berechman, M. Skowronski, and Q. Zhang, J. Appl. Phys. **105**, 074513 (2009).
[13]T. Katsuno, Y. Watanabe, H. Fujiwara, M. Konishi, T. Yamamoto, and T. Endo, Jpn. J. Appl. Phys. **50**, 04DP04 (2011).
[14]H. Fujiwara, M. Konishi, T. Ohnishi, T. Nakamura, K. Hamada, T. Katsuno, Y. Watanabe, T. Endo, T. Yamamoto, K. Tsuruta, and S. Onda, Mater. Sci. Forum **679–680**, 694 (2011).
[15]R. T. Leonard, Y. Khlebnikov, A. R. Powell, C. Basceri, M. F. Brady, I. Khlebnikov, J. R. Jenny, D. P. Malta, M. J. Paisley, V. F. Tsvetkov, R. Zilli, E. Deyneka, H. McD. Hobgook, V. Balakrishna, and C. H. Carter, Jr., Mater. Sci. Forum **600–603**, 7 (2009).
[16]J. Crofton and S. Sriram, IEEE Trans. Electron Devices **43**, 2305 (1996).
[17]M. Treu, R. Rupp, H. Kapels, and W. Bartsch, Mater. Sci. Forum **353–356**, 679 (2001).
[18]C. Blasciuc-Dimitriu, A. B. Horsfall, N. G. Wright, C. M. Johnson, K. V. Vassilevski, and A. G. O'Neill, Semicond. Sci. Technol. **20**, 10 (2005).
[19]R. T. Tung, Phys. Rev. B **45**, 13509 (1992).
[20]J. P. Sullivan, R. T. Tung, M. R. Pinto, and W. R. Graham, J. Appl. Phys. **70**, 7403 (1991).
[21]S. Chand and J. Kumar, J. Appl. Phys. **80**, 288 (1996).
[22]S. Alialy, S. Altindal, E. E. Tanrikulu, and D. E. Yildiz, J. Appl. Phys. **116**, 083709 (2014).
[23]J. Kotani, H. Hasegawa, and T. Hashizume, Appl. Surf. Sci. **237**, 213 (2004).
[24]S. Oyama, T. Hashizume, and H. Hasegawa, Appl. Surf. Sci. **190**, 322 (2002).
[25]G. Krieger and R. M. Swanson, J. Appl. Phys. **52**, 5710 (1981).
[26]B. Majkusiak and A. Jakubowski, J. Appl. Phys. **58**, 3141 (1985).
[27]J. Lutz, H. Schlangenotto, U. Scheuermann, and R. D. Doncker, *Semiconductor Power Devices* (Springer, New York, 2011).
[28]K. J. Schoen, J. M. Woodall, J. A. Cooper, and M. R. Melloch, IEEE Trans. Electron Devices **45**, 1595 (1998).
[29]T. Nakamura, T. Miyanagi, I. Kamata, T. Jikimoto, and H. Tsuchida, IEEE Electron Device Lett. **26**, 99 (2005).
[30]D. Volm, B. K. Meyer, D. M. Hofmann, W. M. Chen, N. T. Son, C. Persson, U. Lindefelt, O. Kordina, E. Sorman, A. O. Konstantinov, B. Monemar, and E. Janzen, Phys. Rev. B **53**, 15409 (1996).
[31]C. Persson and U. Lindefelt, Phys. Rev. B **54**, 10257 (1996).
[32]H. Fujiwara, H. Naruoka, M. Konishi, K. Hamada, T. Katsuno, T. Ishikawa, Y. Watanabe, and T. Endo, Appl. Phys. Lett. **100**, 242102 (2012).
[33]H. Fujiwara, H. Naruoka, M. Konishi, K. Hamada, T. Katsuno, T. Ishikawa, Y. Watanabe, and T. Endo, Appl. Phys. Lett. **101**, 042104 (2012).
[34]G. H. Parker and C. A. Mead, Appl. Phys. Lett. **14**, 21 (1969).
[35]L. Zheng, R. P. Joshi, and C. Fazi, J. Appl. Phys. **85**, 3701 (1999).
[36]M. Furno, F. Bonani, and G. Ghione, Solid-State Electron. **51**, 466 (2007).
[37]F. Roccaforte, F. La Via, V. Raineri, R. Pierobon, and E. Zanoni, J. Appl. Phys. **93**, 9137 (2003).
[38]L. Calcagno, A. Ruggiero, F. Roccaforte, and F. La Via, J. Appl. Phys. **98**, 023713 (2005).
[39]M. E. Aydin, N. Yildirim, and A. Turut, J. Appl. Phys. **102**, 043701 (2007).
[40]A. Sefaoglu, S. Duman, S. Dogan, B. Gurbulak, S. Tuzemen, and A. Turut, Microelectron. Eng. **85**, 631 (2008).
[41]D. Defives, O. Noblanc, C. Dua, C. Brylinski, M. Barthula, V. Aubry-Fortuna, and F. Meyer, IEEE Trans. Electron Devices **46**, 449 (1999).
[42]J. M. Shannon, Appl. Phys. Lett. **24**, 369 (1974).
[43]E. I. Zornberg, Phys. Rev. B **1**, 244 (1970).
[44]C. S. Wang and J. Callaway, Phys. Rev. B **9**, 4897 (1974).
[45]J. B. Goodenough, Phys. Rev. **120**, 67 (1960).
[46]F. M. Steel, B. R. Tuttle, X. Shen, and S. T. Pantelides, J. Appl. Phys. **114**, 013702 (2013).
[47]S. Y. Han and J.-L. Lee, J. Electrochem. Soc. **149**, G189 (2002).
[48]F. Roccaforte, S. Libertino, F. Giannazzo, C. Bongiorno, F. La Via, and V. Raineri, J. Appl. Phys. **97**, 123502 (2005).
[49]F. Roccaforte, F. La Via, A. Raineri, L. Calcagno, and F. Mangano, J. Appl. Phys. **96**, 4313 (2004).
[50]N. W. Ashcroft and N. D. Mermin, *Solid State Physics* (Cengage Learning, Brooks/Cole, Belmont, 1976).
[51]T. Matsumoto, S. Nishizawa, and S. Yamasaki, Mater. Sci. Forum **645–648**, 247 (2010).
[52]R. R. Pawar, Curr. Sci. **36**, 428 (1967).
[53]D. Defives, O. Durand, F. Wyezisk, J. Oliver, O. Noblanc, and C. Brylinski, Mater. Sci. Forum **338–342**, 411 (2000).
[54]A. Kinoshita, T. Nishi, T. Ohyanagi, T. Yatsuo, K. Fukuda, H. Okumura, and K. Arai, Mater. Sci. Forum **600–603**, 643 (2009).
[55]C. R. Crowell, Solid-State Electron. **8**, 395 (1965).